Protein Science (1995), *4*:855-862. Cambridge University Press. Printed in the USA.

Backbone dynamics of the oligomerization domain of p53 determined from ^{15}N NMR relaxation measurements

ROBERT T. CLUBB,[1] JAMES G. OMICHINSKI,[1] KAZUYAZU SAKAGUCHI,[2] ETTORE APPELLA,[2] ANGELA M. GRONENBORN,[1] AND G. MARIUS CLORE[1]

[1] Laboratory of Chemical Physics, Building 5, National Institute of Diabetes and Digestive and Kidney Diseases, National Institutes of Health, Bethesda, Maryland 20892
[2] Laboratory of Cell Biology, Building 37, National Cancer Institute, National Institutes of Health, Bethesda, Maryland 20892

(RECEIVED January 12, 1995; ACCEPTED February 24, 1995)

Abstract

The backbone dynamics of the tetrameric p53 oligomerization domain (residues 319-360) have been investigated by two-dimensional inverse detected heteronuclear ^{1}H-^{15}N NMR spectroscopy at 500 and 600 MHz. ^{15}N T_1, T_2, and heteronuclear NOEs were measured for 39 of 40 non-proline backbone NH vectors at both field strengths. The overall correlation time for the tetramer, calculated from the T_1/T_2 ratios, was found to be 14.8 ns at 35 °C. The correlation times and amplitudes of the internal motions were extracted from the relaxation data using the model-free formalism (Lipari G, Szabo A, 1982, *J Am Chem Soc 104*:4546-4559). The internal dynamics of the structural core of the p53 oligomerization domain are uniform and fairly rigid, with residues 327-354 exhibiting an average generalized order parameter (S^2) of 0.88 ± 0.08. The N- and C-termini exhibit substantial mobility and are unstructured in the solution structure of p53. Residues located at the N- and C-termini, in the β-sheet, in the turn between the α-helix and β-sheet, and at the C-terminal end of the α-helix display two distinct internal motions that are faster than the overall correlation time. Fast internal motions (≤20 ps) are within the extreme narrowing limit and are of uniform amplitude. The slower motions (0.6-2.2 ns) are outside the extreme narrowing limit and vary in amplitude. Four residues at the tetramer interface exhibit a small degree of conformational averaging as evidenced by ^{15}N line broadening, possibly due to sliding or rolling of the helices at the interface of the two dimers that form the tetramer.

Keywords: backbone dynamics; ^{15}N relaxation; p53; solution structure

The p53 protein is a sequence-specific transcriptional activator that plays an important role in tumor suppression (Levine et al., 1991; Lane, 1992; Vogelstein & Kinzler, 1992; Donehower & Bradley, 1993). Inactivation of its tumor suppressor activity, either through mutation or by association with viral or cellular proteins, contributes to the development of as many as 50% of human cancers (Nigro et al., 1989; Takahashi et al., 1989; Hollstein et al., 1991; Harris, 1993). Wild-type p53 controls a cell cycle check point responsible for maintaining genome integrity, inducing cell cycle arrest in response to DNA damage. Tumor-derived mutants are defective in sequence-specific DNA binding activity, suggesting that DNA binding and transcriptional activation are key biochemical activities of p53. Several candidate cellular targets of p53 have been identified including the p21 gene whose function is to inhibit cyclin-dependent kinase-4, thereby blocking cell division at the G_1 checkpoint (El-Deiry et al., 1993; Xiong et al., 1993; Dulic et al., 1994). Transcriptional activation may not be the only function of p53, however, because p53-mediated apoptosis in thymocytes may not require sequence-specific transcriptional activation of genes, but some other functional property of p53 (Caelles et al., 1994).

p53 binds DNA as a tetramer and is composed of four domains: an N-terminal transcriptional activator domain, a central DNA binding domain, an oligomerization domain, and a basic C-terminal nuclear localization domain (Unger et al., 1992; Bargonetti et al., 1993; Pavletich et al., 1993; Prives & Manfredi, 1993; Wang et al., 1993). Although the majority of mutations found in human cancer are located within the DNA binding domain, the oligomerization domain of p53 may also play a key

Reprint requests to: G. Marius Clore or Angela M. Gronenborn, Laboratory of Chemical Physics, Building 5, Room 132, National Institute of Diabetes and Digestive and Kidney Diseases, National Institutes of Health, Bethesda, Maryland 20892; e-mail: clore@vger.niddk.nih.gov or gronenborn@vger.niddk.nih.gov.

role in cell transformation. This region is believed to be responsible for the dominant negative phenotypes of certain p53 mutations because heterotetramers of mutant and wild-type p53 are either unable to bind DNA sequence specifically or bind with significantly reduced affinity, thereby reducing the efficiency of p53-dependent gene activation. A single mutated allele of p53 may therefore decrease the probability that damage to the genome will be repaired before cell division.

The structure of the p53 oligomerization domain has recently been determined by NMR (Clore et al., 1994, 1995a, 1995b; Lee et al., 1994) and crystallography (Jeffrey et al., 1995). This domain forms a ~20-kDa symmetrical tetramer and is comprised of a four-helix bundle with two antiparallel β-sheets located on opposing faces of the molecule. This structure in conjunction with the recently determined co-crystal structure of the central domain of p53 bound to DNA (Cho et al., 1994) has provided a structural framework with which to interpret the significance of tumor-derived mutants of p53.

In order to obtain a more comprehensive picture of the p53 oligomerization domain, we have characterized its internal mobility using inverse detected ^1H-^{15}N two-dimensional heteronuclear NMR spectroscopy (reviewed in Peng & Wagner, 1994). ^{15}N T_1, T_2, and NOE data at 500- and 600-MHz field strengths were determined for 39 amide groups and analyzed using the model-free formalism of Lipari and Szabo in both its original (Lipari & Szabo, 1982) and extended (Clore et al., 1990b) forms. All residues exhibit very fast motions on time scales $\leq$20 ps, and 15 residues display a second slower motion on a time scale of 0.6–2.2 ns; finally, four residues at the helical interface undergo motions on time scales ranging between about 30 ns and 10 ms.

Results

^{15}N relaxation data were collected at 35 °C at two field strengths (500 and 600 MHz). Spectra of the p53 oligomerization domain (residues 319–360) were assigned using previously published resonance assignments (Clore et al., 1994). The p53 oligomerization domain is a symmetric tetramer composed of a dimer of dimers (Clore et al., 1994, 1995a, 1995b). The quality of the spectra is illustrated in Figure 1, which shows the ^{15}N-^1H NOE correlation spectrum (with proton saturation) of the p53 oligomerization domain. The majority of residues exhibit positive NOEs (Fig. 1A); several residues, however, at the N- and C-termini of the tetramer (Lys 319, Lys 321, Lys 357, and Gly 360) exhibit negative NOEs, suggesting significant mobility (Fig. 1B). Although the molecular weight of the oligomerization domain is ~20 kDa, molecular symmetry results in a very simple NMR spectrum and the relaxation behavior of 39 of the 40 non-proline residues could be monitored. ^{15}N T_1 and T_2 values were determined from exponential fits of the crosspeak intensities in 2D ^1H-^{15}N relaxation spectra as a function of delay time. Representative fits of the ^{15}N T_1 and T_2 decay curves are shown in Figure 2A and B, respectively. Typically, the fitting errors for the ^{15}N T_1 and T_2 data curves at both field strengths were <1%. A summary of the measured ^{15}N T_1, T_2, and NOE data, plotted as a function of residue number, is shown in Figure 3A, B, and C, respectively. In general, the data indicate that the p53 oligomerization domain has uniform mobility within the central portion of its amino acid sequence (residues 327–354) but exhibits large amplitude motions at its N- and C-termini.

^{15}N T_1/T_2 ratios were used to determine the overall correlation time of the oligomerization domain (Kay et al., 1989; Clore et al., 1990a). The average T_1/T_2 ratio for all residues in the tetramer was 12.36 ± 5.66 and 15.98 ± 7.85 at 500 and 600 MHz, respectively. The overall correlation time, τ_r, was obtained by fitting the T_1 and T_2 data of 16 residues that satisfied the following criteria: (1) the residues had NOE values >0.6 at both 500 and 600 MHz; (2) the residues were within ±1 SD of the average T_1/T_2 ratio of residues satisfying criteria (1). The T_1/T_2 ratios of these 16 residues was 16.08 ± 0.60 and 21.23 ± 1.20, at 500 and 600 MHz, respectively. The overall correlation time for the p53 tetramer calculated from these data was 14.82 ± 0.08 ns.

The ^{15}N NOE, T_1, and T_2 data for each residue were fit simultaneously to various forms of model-free spectral density function (Lipari & Szabo, 1982), in the presence or absence of an additional term ($\pi\Delta ex$), to account for the effects of chemical exchange line broadening on T_2 (Clore et al., 1990a). In the model-free analysis, the overall motion of the protein is assumed to be isotropic and the internal motions are considered to be independent of the overall tumbling. This approximation appears reasonable because the three principle components of the inertia tensor for the average solution structure of the p53 oligomer-

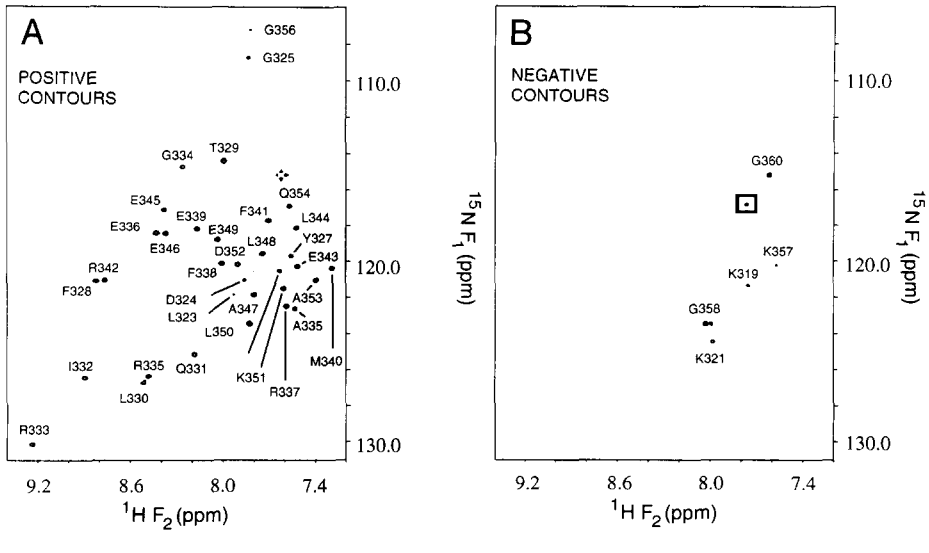

Fig. 1. ^{15}N-^1H NOE correlation spectrum at 600 MHz of the oligomerization domain of p53 plotted with positive (**A**) and negative (**B**) contours, respectively. Boxed crosspeak in B is an unassigned artifact.

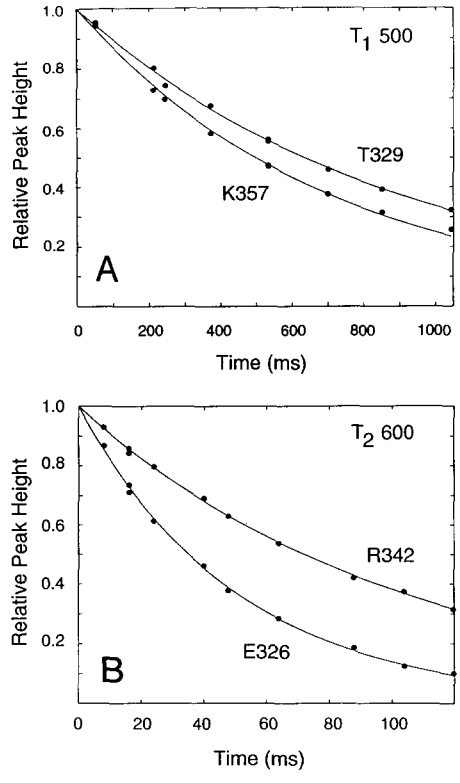

Fig. 2. Representative plots of crosspeak intensity versus delay time of the T_1 data at 500 MHz (**A**) and T_2 data at 600 MHz (**B**).

ization domain (Clore et al., 1995b) are in a ratio of 1.00:1.29:1.60, indicative of an approximately globular structure.

The spectral density functions used to fit the relaxation data differ in the degree of complexity assumed for the internal motions and consequently in the number of adjustable parameters used to reproduce the experimental data. Three models, containing one to three adjustable parameters, were used to fit the data. Selection of the appropriate spectral density function was accomplished by initially fitting the data to the simplest spectral density function and only employing more complicated models as required to fit the relaxation data. The experimental data for a residue were considered to be adequately represented by a particular spectral density function if the T_1 and T_2 data were reproduced to within 5% and the NOE data to within ±0.1 of their experimentally determined values. Because all experimental relaxation parameters (i.e., T_1, T_2, and NOE at 500 and 600 MHz) were fit simultaneously for each residue, we typically found that spectral density functions that did not fit the experimental data failed to adequately account for all relaxation parameters, rather than only one type of relaxation parameter.

The data for 12 of the 39 measurable backbone amide groups could be accounted for by a simplified model-free spectral density function, $J(\omega_i)$, in which the internal correlation time, τ_e, is assumed to be less than 20 ps and therefore makes an insignificant contribution to $J(\omega_i)$:

$$J(\omega_i) = S^2\tau_r/(1 + \omega^2\tau_r^2), \quad (1)$$

where S^2 is the generalized overall order parameter (Lipari & Szabo, 1982). The spectral density function of Equation 1 results in the maximum value of the calculated NOE for a given τ_r. For a rotational correlation time of 14.8 ns, the theoretical NOE maxima are 0.830 and 0.813 at spectrometer frequencies of 600 and 500 MHz, respectively. The data for six residues necessitated the use of the complete model-free spectral density function of Lipari and Szabo (1982):

$$J(\omega_i) = S^2\tau_r/(1 + \omega^2\tau_r^2) + (1 - S^2)\tau_e'/(1 + \omega^2\tau_e'^2), \quad (2)$$

where $\tau_e' = \tau_r\tau_e/(\tau_r + \tau_e)$, and τ_e is the internal correlation time. The calculated τ_e for these residues ranged from 26 to 57 ps with relative error estimates ranging from 40 to 15%. The data for 15 residues could not be fit with Equation 2 (typically their NOE and T_1 values were not adequately reproduced). These residues required the use of the extended model-free spectral density function (Clore et al., 1990b):

$$J(\omega_i) = S^2\tau_r/(1 + \omega^2\tau_r^2) + S_f^2(1 - S_s^2)\tau_s'/(1 + \omega^2\tau_s'^2), \quad (3)$$

where S_f^2 and S_f^2 are the order parameters for the fast and slow motions, respectively, and τ_s is the internal correlation time for the slow motions (with $\tau_s' = \tau_r\tau_s/(\tau_r + \tau_s)$). The terms containing τ_f are neglected because the internal correlation time for the fast motions, τ_f, is assumed to be less than 20 ps. The values of τ_s ranged from ~0.6 to ~2.2 ns and are displayed in Figure 3F.

Four residues (Glu 343, Ala 347, Leu 348, and Leu 351) are likely to exhibit chemical exchange line broadening because they have T_1/T_2 ratios (at both 500 and 600 MHz) that are one standard deviation above the mean T_1/T_2 ratio of residues with NOE values >0.6. The effect of chemical exchange line broadening on T_2 is described by:

$$1/T_2(obs) = 1/T_2 + \pi\Delta ex, \quad (4)$$

where Δex is the increase in the ^{15}N linewidth as a result of chemical exchange, and $T_2(obs)$ and T_2 are the observed and actual transverse relaxation times, respectively. If the exchange is fast on the chemical shift time scale, the chemical exchange terms at the two spectrometer frequencies are related by:

$$\pi\Delta ex(500) = \pi\Delta ex(600) \times 0.694, \quad (5)$$

and only one chemical exchange term needs to be optimized (Barchi et al., 1994). The relaxation data for Ala 347, Leu 348, and Leu 351 were adequately reproduced using the simplest model-free spectral density function and a single T_2 exchange term (Equations 1, 4, 5). The ^1H-^{15}N correlation of Glu 343 is partially overlapped with Lys 357. Nevertheless, the T_1 and NOE data of this residue were fit to within the specified limits, and the T_2 data could be reproduced to within 7.8 and 8.1% of the experimentally determined values at 500 and 600 MHz, respectively.

Finally, the data for Lys 319 and Gly 360 could not be reproduced to within our defined limits and are located at the unstructured termini of the p53 oligomerization domain (Clore et al., 1994, 1995a, 1995b). Analysis of the residuals for Lys 319 indicated that the extended model-free spectral density function of Equation 3 best fit the experimental data; the calculated T_2 data at 600 MHz and 500 MHz were within 5.9% and 5.7% of the experimental values, respectively. The data for Gly 360, however, could not be reproduced by any of the models described

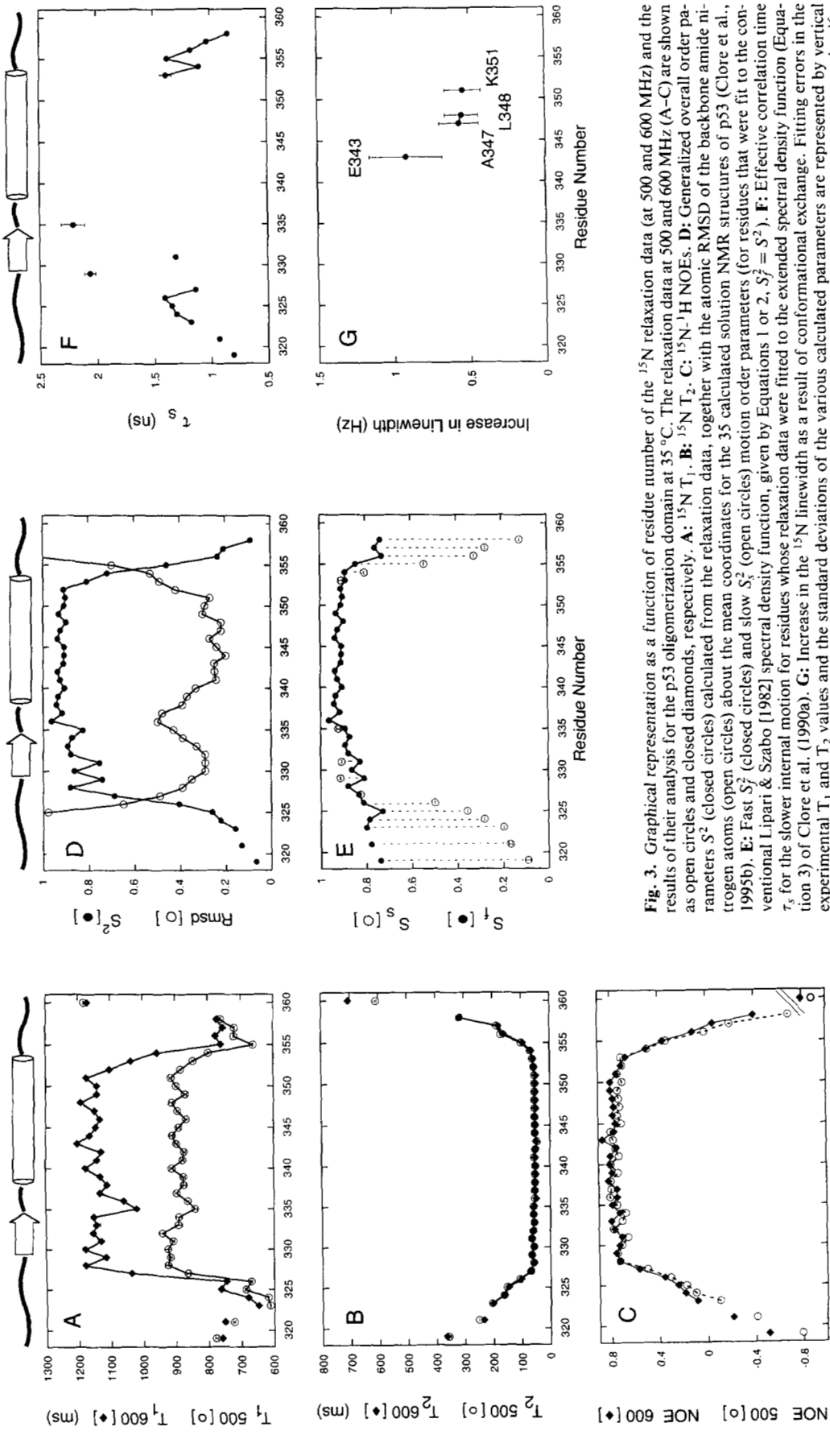

Fig. 3. *Graphical representation as a function of residue number of the* ^{15}N relaxation data (at 500 and 600 MHz) and the results of their analysis for the p53 oligomerization domain at 35 °C. The relaxation data at 500 and 600 MHz (A–C) are shown as open circles and closed diamonds, respectively. **A:** ^{15}N T_1. **B:** ^{15}N T_2. **C:** ^{15}N-^1H NOEs. **D:** Generalized overall order parameters S^2 (closed circles) calculated from the relaxation data, together with the atomic RMSD of the backbone amide nitrogen atoms (open circles) about the mean coordinates for the 35 calculated solution NMR structures of p53 (Clore et al., 1995b). **E:** Fast S_f^2 (closed circles) and slow S_s^2 (open circles) motion order parameters (for residues that were fit to the conventional Lipari & Szabo [1982] spectral density function, given by Equations 1 or 2, $S_f^2 = S^2$). **F:** Effective correlation time τ_s for the slower internal motion for residues whose relaxation data were fitted to the extended spectral density function (Equation 3) of Clore et al. (1990a). **G:** Increase in the ^{15}N linewidth as a result of conformational exchange. Fitting errors in the experimental T_1 and T_2 values and the standard deviations of the various calculated parameters are represented by vertical bars. In the majority of cases the size of these errors is smaller than that of the symbols. Errors in the experimental ^1H-^{15}N NOEs are on the order of ±0.1. Locations of the β-strand and α-helix are indicated above each set of panels.

by Equations 1, 2, and 3, and probably undergo very complicated motions.

The results of the data analysis are summarized in Figure 3D, E, F, and G, which shows plots of the values of the various optimized parameters as a function of residue number. These parameters include the overall generalized order parameter (Fig. 3D), the fast and slow order parameters (Fig. 3E), correlation times characterizing the slower motional process (Fig. 3F), and the increase in ^{15}N line widths as a result of conformational averaging (Fig. 3G).

Discussion

The rotational correlation time of 14.8 ns for the tetrameric p53 oligomerization domain (residues 319–360) is larger than those reported for proteins of similar molecular weight for which ^{15}N relaxation data have been reported (Kay et al., 1989; Clore et al., 1990a; Barbato et al., 1992; Stone et al., 1992). However, it is only slightly larger than the value reported for human granulocyte colony-stimulating factor (MW = 18.9 kDa, $\tau_r = 12.1$ ns) (Zink et al., 1994), which is also composed of a four-helix bundle. In this regard, it is important to note that the rotational correlation time is dependent on the radius of the protein rather than on the molecular weight. The large observed τ_r value for the p53 oligomerization domain can be directly attributed to the large value of 19.2 Å calculated for the radius of gyration of the tetramer (Clore et al., 1995a, 1995b), which arises from the protrusion of eight symmetrically related, disordered polypeptide termini, 8 and 6 residues in length at the N- and C-termini, respectively (Fig. 4A,B). If these tails are excluded, the calculated radius of gyration is 14.4 Å and the molecular weight is about 13 kDa. As the rotational correlation time is proportional to the cube of the radius, this translates to an expected correlation time of 6.1 ns for the core of the oligomerization domain (residues 327–354), which is exactly what one would expect for a 13-kDa globular protein. It is also instructional to calculate the expected ^{15}N T_1 and T_2 values for different correlation times, assuming only fast restricted internal motions with typical values of $S^2 = 0.85$ and $\tau_e = 10$ ps. For an overall correlation time of 14.8 ns, this yields ^{15}N T_1 values of ~940 and 1,230 ms at 500 and 600 MHz, respectively, and T_2 values of ~60 ms at both field strengths. Examination of the data in Figure 3A and B shows that the experimental ^{15}N T_1 and T_2 values for residues in the structured core have values that are consistent with these estimates. Thus, residues with ^1H-^{15}N NOE values greater than 0.6 have average observed ^{15}N T_1 values of 893 ± 25 ms and 1,137 ± 45 ms at 500 and 600 MHz, respectively, and average observed ^{15}N T_2 values of 56 ± 4 ms and 54 ± 5 ms at 500 and 600 MHz, respectively. For an overall correlation time of 9 ns, on the other hand, which would be expected for an ~20-kDa globular protein with no symmetrically placed floppy tails, the expected ^{15}N T_1 values would be 610 and 790 ms at 500 and 600 MHz, respectively, and the expected ^{15}N T_2 values would be ~90 ms at both field strengths. Thus, the experimentally observed ^{15}N T_1 and T_2 values for the core residues are approximately 50% larger and 35% smaller, respectively, than the expected values for a 9-ns rotational correlation time.

Nonspecific aggregation could also increase the observed rotational correlation time of the p53 tetramer, but this is unlikely because the $^1H^N$ line widths appear to be nearly independent of protein concentration. In principle, uniform conformation ex-

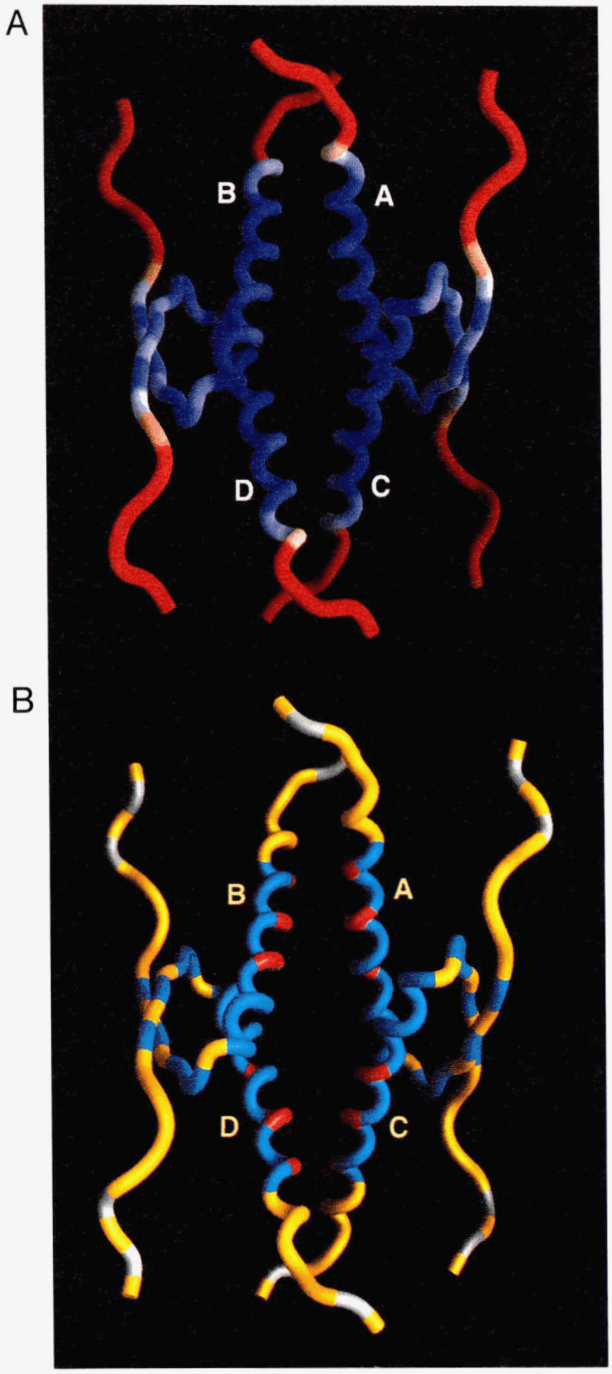

Fig. 4. Ribbon diagram of the backbone of the p53 oligomerization domain color coded (**A**) to display the variation in the generalized order parameter S^2 varying from blue (low mobility and $S^2 \sim 1.0$) through white ($S^2 \sim 0.66$) to red (high mobility and $S^2 \sim 0.27$), and (**B**) to indicate the spectral density functions and chemical exchange properties of the different residues. The color coding in B is as follows: blue, residues whose relaxation data could be fitted to the Lipari and Szabo (1982) spectral density functions given by Equations 1 or 2; red, Equation 1 plus a chemical exchange term (Equations 4, 5); yellow, extended spectral density function of Equation 3 (Clore et al., 1990b); and gray, proline residues and Lys 320, for which ^{15}N relaxation data could not be measured. Coordinates are taken from Clore et al. (1995b), PDB accession number 10LG. The interhelical angles and the orientation of the two dimers in this structure are the same as those in the X-ray structure (Clore et al., 1995b; Jeffrey et al., 1995). Figures were generated with the program GRASP (Nicholls et al., 1991).

change processes could potentially result in an overestimate of τ_r. Analysis of Figure 3B reveals that, with the exception of the C-terminal tail of p53 (Gly 360), the ^{15}N T_2 values at 500 and 600 MHz are essentially independent of spectrometer frequency. Therefore, no detectable uniform conformational exchange processes can be occurring in the p53 tetramer.

The results of the relaxation data analysis can best be interpreted by mapping them onto the solution structure of the oligomerization domain of p53. Figure 4A displays the variation of the generalized order parameter (S^2) as a color gradient from red (highly mobile) to blue (low mobility) on a ribbon diagram of the three-dimensional structure. Clearly, residues at the tetramer interface exhibit an increased degree of motional restriction. The structure of the p53 tetramer (Fig. 4A,B) is comprised of a turn from Asp 324 to Glu 326, a β-strand from Glu 326 to Gly 334, a turn from Gly 334 to Arg 335, and finally an α-helix from Arg 335 to Ala 355. The structure comprises a dimer of dimers. Each dimer is composed of an antiparallel β-sheet that lies on the outside of the whole molecule, and two antiparallel α-helices that form the interface between the two dimers. The tetramer comprises a four-helix bundle with the two dimers arranged approximately orthogonal (80°) to each other (Clore et al., 1995a, 1995b). The p53 core exhibits fairly rigid internal dynamics, with residues 327–354 exhibiting generalized order parameters (S^2) greater than 0.68 and an average S^2 value of 0.88 ± 0.08. Residues in the turn preceding the β-sheet (324–325), the first two residues in the β-sheet (326–327), and two residues at the C-terminal end of the α-helix (354–355) are more mobile than the core. The N- and C-termini of the monomers of the p53 tetramer are significantly more mobile, with average S^2 values of 0.17 ± 0.08 and 0.21 ± 0.08, for residues 319–325 and 356–358, respectively.

Interestingly, the secondary structural elements of the p53 tetramer undergo varying amounts of internal motion. Analysis of Figures 3D and 4A reveal that the α-helices at the interface of the two dimers exhibit uniform low-amplitude fast motions between residues 337 to 353, with an average S^2 value of 0.91 ± 0.03. The residues of the β-sheet exhibit nonuniform internal dynamics and are more mobile than the α-helix, with an average S^2 value of 0.78 ± 0.2. The degree of internal mobility within the β-sheet depends on the orientation of the NH vectors and whether it is involved in interstrand hydrogen bonds. Amide groups that participate in interstrand backbone hydrogen bonds (Phe 328, Leu 330, Ile 332, and Gly 334) have restricted mobility, with an average S^2 value of 0.88 ± 0.01. The NH vectors of residues not involved in secondary structure hydrogen bonds (Thr 329, Gln 331, and Arg 333), on the other hand, are more mobile with S^2 values of 0.73 ± 0.03.

The generalized order parameters (S^2) and the average atomic RMS deviation (RMSD) of the 35 calculated NMR structures about their mean coordinate positions (Clore et al., 1995b) are inversely correlated at the N- and C-termini of the protein. The RMSD values of the backbone nitrogen atoms increase for residues at the N- and C-termini, whereas the S^2 values of these residues progressively decrease as the ends of the polypeptide chain are approached. There is only a weak inverse relationship within the core of p53, with residues in the β-sheet exhibiting slightly larger RMSD values and generally lower and more variable generalized order parameters. There is no correlation between the RMSD and S^2 values of residues in the turn connecting the β-sheet and α-helix. Gly 334 and Arg 335 exhibit larger than average RMSD values (0.41 ± 0.03) but have average S^2 values (0.85 ± 0.03; Gly 334–Arg 335). Furthermore, a nearby residue, Glu 336, exhibits the largest RMSD value within the core (0.50 Å) but has an above average order parameter ($S^2 = 0.95$), indicative of restricted internal motion. These results are not surprising because the RMSD values depend on the number and distribution of interproton restraints, which are only indirectly related to the internal dynamics of the protein and more importantly, directly related to the packing density of nearby protons (Powers et al., 1993).

The relaxation data of several residues could only be accounted for by the extended spectral density function of Equation 3 (Clore et al., 1990a, 1990b). Figure 3E displays a plot of the fast S_f^2 and slow S_s^2 order parameters versus sequence number (note that for residues fit with Equations 1 or 2, $S^2 = S_f^2$). Residues that require the extended spectral density function of Equation 3 exhibit uniform fast internal motions with slower motions of variable amplitude. As shown in Figure 4B, residues that undergo motions on time scales ranging from 0.6 to 2.2 ns are located at the N- and C-termini of the protein, in the β-sheet (Thr 329 and Gln 331), in the turn between the helix and sheet (Arg 335), and at the C-terminal end of the helix (Ala 353). The simplest physical model for these motions is one in which the slow motion is represented by a jump between two states, i and j, where the fast librational motion is represented as free diffusion within two axially symmetric cones, centered about the two states i and j (Clore et al., 1990a). The correlation times for these slow motional processes are plotted in Figure 3G, and range from 810 ps (Lys 319) to 2.2 ns (Arg 335). Molecular dynamics simulations suggest that the slow motions may involve large-amplitude jumps between well-defined orientations that are stabilized by hydrogen bonds (Chandrasekhar et al., 1992; Eriksson et al., 1993).

Analysis of Figure 3F reveals that the values of the motional parameter, τ_s, are well determined by the experimental relaxation data, suggesting that the relaxation data of these residues is best interpreted with the extended model-free formalism depicted by Equation 3 (Clore et al., 1990b). In order to verify this conclusion the p53 relaxation data were also fit with the spectral density function of Equation 2 and the values of τ_e analyzed. As expected, nearly all residues that required Equation 3 to fit their experimental data exhibited τ_e values outside the extreme narrowing limit when fitted to Equation 2, indicating that they experience internal motions on a time scale between 1 and 3 ns. The data for three residues were exceptional and did not exhibit τ_e values outside the extreme narrowing range when fit with Equation 2 (Thr 329, $\tau_e = 31$ ps; Gln 331, $\tau_e = 46$ ps; Arg 335, $\tau_e = 84$ ps). However, the agreement with the experimental data using the model of Equation 2 fell outside our defined limits (all three residues have at least two relaxation parameters that were not fit to within <5% of the T_1 and T_2 and values within ±0.1 of their NOEs). Therefore, although the experimental data of Thr 329, Gln 331, and Arg 335 are best reproduced by the extended spectral density function (Equation 3), the presence of a slow motional process is not necessarily an inherent feature of their relaxation data.

The relaxation data suggest that four residues have internal motions on time scales ranging from 170 ns to 2.25 ms (Powers et al., 1992). These residues are located at the interface of the two dimers formed by residues at the C-terminal end of the α-helix (Glu 343, Ala 347, Leu 348, and Lys 351) and are col-

ored orange in Figure 4B. The magnitude of these processes (Fig. 3G) is relatively small, with a maximum increase in the ^{15}N linewidth of 0.92 ± 0.24 Hz at 600 MHz (Glu 343) and a mean value of 0.65 ± 0.18 Hz. These motions must involve at least two species with different chemical shifts. However, because the number of distinct species and the chemical shift differences are unknown, no estimation of the rates of these processes can be ascertained. Furthermore, the experimental data afford no information on the magnitude of these motions. The possible origin of this effect may reside in the sliding or rolling of the helices at the dimer–dimer interface.

Concluding remarks

We have characterized the backbone dynamics of the p53 oligomerization domain (residues 319–360) by analysis of ^{15}N relaxation data at two field strengths. Our results indicate that the p53 oligomerization domain is comprised of two distinct regions, a central core formed by residues 327–354, which exhibits restricted internal motions, and eight flexible tails that undergo complicated unrestricted motions. The structured core itself exhibits variable internal mobility and can be divided into two regions, a central rigid four-helical bundle that exhibits uniformly restricted fast internal motions, and a more flexible β-sheet region, which exhibits less uniform internal mobility. Although the internal dynamics at the helical interface are rigid on the picosecond to nanosecond time scales, observed ^{15}N line broadening in the four-helical bundle suggests that a slow nanosecond to millisecond process exists. We suggest that the observed line broadening may be due to fluctuating motions caused by sliding or rolling of the helices at the interface of the two dimers that forms the tetramer.

Materials and methods

The p53 oligomerization peptide was uniformly (>95%) ^{15}N labeled, and purified as described previously (Clore et al., 1994). The sample for NMR contained 5.0 mM peptide in 90% H_2O/10% D_2O, pH 6.8. Experiments were performed at both 500 and 600 MHz on Bruker AMX-500 and -600 spectrometers equipped with actively shielded *z*-gradient triple resonance probes and gradient amplifier units.

The ^{15}N relaxation data were obtained as described previously (Kay et al., 1989; Clore et al., 1990a; Grasberger et al., 1993; Barchi et al., 1994). Solvent signal suppression was obtained by application of a WATERGATE sequence (Piotto et al., 1992) and appropriately placed purge pulses (Messerle et al., 1989). All experiments employed pulse field gradients for artifact suppression (Bax & Pochapsky, 1992; Keeler et al., 1994). The heteronuclear NOE measurements used the water "flip-back" method to avoid saturation of the amide resonances (Grzesiek & Bax, 1993). All experiments utilized a total of 1,024 and 140 complex points in $F_2(^1H)$ and $F_1(^{15}N)$, respectively. The ^1H and ^{15}N carriers were positioned at 4.68 ppm and 118.5 ppm, respectively. ^1H sweep widths of 6,024.10 and 9,259.26 Hz were used at 500 and 600 MHz, respectively. ^{15}N sweep widths of 1,366.12 and 1,524.39 Hz were used at 500 and 600 MHz, respectively. The recycle time was 1.5 s for the ^{15}N T_1 and T_2 experiments, and 3.0 s for the NOE experiments.

^{15}N T_2 values (at 500 and 600 MHz) were obtained using delays of 8, 16 (two experiments), 24, 40, 48, 64, 88, 104, 120, and 176 ms. Seven experiments were recorded at 600 MHz to measure ^{15}N T_1 values and utilized delays of 52, 212, 244, 372, 532, 700, and 852 ms. ^{15}N T_1 measurements at 500 MHz were recorded with delays of 52, 212, 244, 372, 532 (two experiments), 700, 852, and 1,044 ms. Crosspeak intensities were determined by time domain simulation of the data using in-house software (F. Delaglio, unpubl. data). The decays of the derived crosspeak intensities with time in the ^{15}N T_1 and T_2 experiments were fit to a single exponential by nonlinear least-squares methods. Fitting errors of the T_1 and T_2 values were typically less than 1%. The errors in the NOE measurements were on the order of ±0.1. Model-free parameters were determined by nonlinear least-squares minimization of the sum of the error-weighted residuals between the calculated and experimental data using the Levenburg–Marquardt algorithm (Press et al., 1986). Precision estimates of the extracted model-free parameters were obtained by the Monte Carlo approach as described by Kamath and Shriver (1989).

Acknowledgments

We thank N. Tjandra, F. Delaglio, and S. Grzesiek for many useful discussions; R. Tschudin for technical support; F. Delaglio and D.S. Garrett for writing the NMR processing and analysis software, respectively; and J. Ernst for generating Figure 4. This work was supported by a Leukemia Society of America postdoctoral fellowship (to R.T.C.) and the AIDS Targeted Antiviral Program of the Office of the Director of the National Institutes of Health (to G.M.C., A.M.G., and E.A.).

References

Barbato G, Ikura M, Kay LE, Pastor RW, Bax A. 1992. Backbone dynamics of calmodulin studied by ^{15}N relaxation using inverse detected two-dimensional NMR spectroscopy: The central helix is flexible. *Biochemistry 31*:5269–5278.

Barchi JJ, Grasberger BL, Gronenborn AM, Clore GM. 1994. Investigation of the backbone dynamics of the IgG-binding domain of streptococcal protein G by heteronuclear two-dimensional ^1H-^{15}N nuclear magnetic resonance spectroscopy. *Protein Sci 3*:15–21.

Bargonetti J, Manfredi JJ, Chen X, Marshak DR, Prives C. 1993. A proteolytic fragment from the central region of p53 has marked sequence-specific DNA-binding activity when generated from wild-type but not from oncogenic mutant p53. *Genes & Dev 7*:2565–2574.

Bax A, Pochapsky SS. 1992. Optimized recording of heteronuclear multidimensional NMR spectra using pulsed field gradients. *J Magn Reson 99*:638–643.

Caelles C, Helmberg A, Karin M. 1994. p53-dependent apoptosis in the absence of transcriptional activation of p53-target genes. *Nature 370*: 220–223.

Chandrasekhar I, Clore GM, Szabo A, Gronenborn AM, Brooks BR. 1992. A 500 ps molecular dynamics simulation study of interleukin-1β in water: Correlation with nuclear magnetic resonance spectroscopy and crystallography. *J Mol Biol 226*:239–250.

Cho Y, Gorina S, Jeffrey PD, Pavletich NP. 1994. Crystal structure of a p53 tumor suppressor–DNA complex: Understanding tumorigenic mutations. *Science 265*:346–355.

Clore GM, Driscoll PC, Wingfield PT, Gronenborn AM. 1990a. Analysis of the backbone dynamics of interleukin-1β using two-dimensional inverse detected heteronuclear ^{15}N-^1H NMR spectroscopy. *Biochemistry 29*:7387–7401.

Clore GM, Ernst J, Clubb R, Omichinski JG, Sakaguchi K, Appella E, Gronenborn AM. 1995a. Refined solution structure of the oligomerization domain of the tumour suppressor p53. *Nature Struct Biol 2*:321–338.

Clore GM, Omichinski JG, Sakaguchi K, Zambrano N, Sakamoto H, Appella E, Gronenborn AM. 1994. High-resolution structure of the oligomerization domain of p53 by multidimensional NMR. *Science 265*: 386–391.

Clore GM, Omichinski JG, Sakaguchi K, Zambrano N, Sakamoto H, Appella E, Gronenborn AM. 1995b. Interhelical angles in the solution

structure of the oligomerization domain of the tumour suppressor p53. *Science 267*:1515-1516.

Clore GM, Szabo A, Bax A, Kay LE, Driscoll PC, Gronenborn AM. 1990b. Deviations from the simple two-parameter model-free approach to the interpretation of nitrogen-15 nuclear magnetic relaxation of proteins. *J Am Chem Soc 112*:4989-4991.

Donehower LA, Bradley A. 1993. The tumor suppressor p53. *Biochim Biophys Acta 1155*:181-205.

Dulic V, Kaufmann WK, Wilson SJ, Tlsty TD, Lees E, Harper JW, Elledge SJ, Reed SI. 1994. p53-dependent inhibition of cyclin-dependent kinase activities in human fibroblasts during radiation-induced G1 arrest. *Cell 76*:1013-1023

El-Deiry WS, Tokino T, Velculescu VE, Levy DB, Parsons R, Trent JM, Lin D, Mercer WE, Kinzler KW, Vogelstein B. 1993. WAF1, a potential mediator of p53 tumor suppression. *Cell 75*:817-825.

Eriksson MAL, Berglund H, Hard T, Nilsson L. 1993. A comparison of ^{15}N NMR relaxation measurements with a molecular dynamics simulation: Backbone dynamics of the glucocorticoid receptor DNA-binding domain. *Proteins Struct Funct Genet 17*:375-390.

Grasberger BL, Gronenborn AM, Clore GM. 1993. Analysis of the backbone dynamics of interleukin-8 by ^{15}N relaxation measurements. *J Mol Biol 230*:364-372.

Grzesiek S, Bax A. 1993. The importance of not saturating H_2O in protein NMR. Application to sensitivity enhancement and NOE measurements. *J Am Chem Soc 115*:12593-12594.

Harris CC. 1993. p53: At the crossroads of molecular carcinogenesis and risk assessment. *Science 262*:1980-1981.

Hollstein M, Sidransky B, Vogelstein B, Harris CC. 1991. p53 mutations in human cancers. *Science 253*:49-53.

Jeffrey PD, Gorina S, Pavletich NP. 1995. Crystal structure of the tetramerization domain of the p53 tumour suppressor at 1.7 Å. *Science 267*:1498-1502.

Kamath U, Shriver JW. 1989. Characterization of thermotropic state changes in myosin subfragment-1 and heavy meromyosin by UV differences spectroscopy. *J Biol Chem 264*:5586-5592.

Kay LE, Torchia DA, Bax A. 1989. Backbone dynamics of proteins as studied by ^{15}N inverse detected heteronuclear NMR spectroscopy: Application to staphylococcal nuclease. *Biochemistry 28*:8972-8979.

Keeler J, Clowes RT, Davis AL, Laue ED. 1994. Pulsed-field gradients: Theory and practice. *Methods Enzymol 239*:145-207.

Lane DP. 1992. p53, guardian of the genome. *Nature 358*:15-16.

Lee W, Harvey TS, Yin Y, Yau P, Litchfield D, Arrowsmith CH. 1994. Solution structure of the tetrameric minimum transforming domain of p53. *Nature Struct Biol 1*:877-890.

Levine AJ, Momand J, Finlay CA. 1991. The p53 tumor suppressor gene. *Nature 351*:453-456.

Lipari G, Szabo A. 1982. Model-free approach to the interpretation of nuclear magnetic resonance relaxation in macromolecules. 1. Theory and range of validity. *J Am Chem Soc 104*:4546-4559.

Messerle BA, Wider G, Otting G, Weber C, Wüthrich K. 1989. Solvent suppression using a spin lock in 2D and 3D NMR spectroscopy with H_2O solutions. *J Magn Reson 85*:608-613.

Nicholls A, Sharp KA, Honig B. 1991. Protein folding and association: Insights from the interfacial and thermodynamic properties of hydrocarbons. *Proteins Struct Funct Genet 11*:281-296.

Nigro JM, Baker SJ, Preisinger AC, Jessup JM, Hostetter R, Leary K, Bigner SH, Davidson N, Baylin S, Devilee P, Glover T, Collins FS, Weston A, Modali R, Harris CC, Vogelstein B. 1989. Mutations in the p53 gene occur in diverse human tumour types. *Nature 342*:705-708.

Pavletich NP, Chambers KA, Pabo CO. 1993. The DNA-binding domain of p53 contains the four conserved regions and the major mutation hot spots. *Genes & Dev 7*:2556-2564.

Peng JW, Wagner G. 1994. Investigations of protein motions via relaxation measurements. *Methods Enzymol 289*:563-596.

Piotto M, Saudek V, Sklenar V. 1992. Gradient-tailored excitation for single-quantum NMR spectroscopy of aqueous solutions. *J Biomol NMR 2*: 661-665.

Powers R, Clore GM, Garrett DS, Gronenborn AM. 1993. Relationships between the precision of high resolution protein NMR structures, solution order parameters, and crystallographic B factors. *J Magn Reson Ser B 101*:325-327.

Powers R, Clore GM, Stahl SJ, Wingfield PT, Gronenborn AM. 1992. Analysis of the backbone dynamics of the ribonuclease H domain of the human immunodeficiency virus reverse transcriptase using ^{15}N relaxation measurements. *Biochemistry 31*:9150-9157.

Press WH, Flannery BP, Teukolsky SA, Vetterling WT. 1986. *Numerical recipes in C*. Cambridge, UK: Cambridge University Press.

Prives C, Manfredi JJ. 1993. The p53 tumor suppressor protein: Meeting review. *Genes & Dev 7*:2556-2564.

Stone MJ, Fairbrother WJ, Palmer AG, Reizer J, Saier MH, Wright PE. 1992. Backbone dynamics of the *Bacillus subtilis* glucose permease IIA domain determined from ^{15}N NMR relaxation measurements. *Biochemistry 31*:4394-4406.

Takahashi T, Nau MM, Chiea I, Birrer MJ, Rosenberg RK, Vinocour M, Levitt M, Pass H, Gazdar AF, Minna JD. 1989. p53: A frequent target for genetic abnormalities in lung cancer. *Science 246*:491-494.

Unger T, Nau MM, Segal S, Minna JD. 1992. p53: A transdominant regulator of transcription whose function is ablated by mutations occurring in human cancer. *EMBO J 11*:1383-1390.

Vogelstein B, Kinzler KW. 1992. p53 function and dysfunction. *Cell 70*: 523-526.

Wang Y, Reed M, Wang P, Stenger JE, Mayr G, Anderson ME, Schwedes JF, Tegtmeyer P. 1993. p53 domains: Identification and characterization of two autonomous DNA-binding domains. *Genes & Dev 7*:2575-2586.

Xiong Y, Hannon GJ, Zhang H, Casso D, Kobayashi R, Beach D. 1993. p21 is a universal inhibitor of cyclin kinases. *Nature 366*:701-704.

Zink T, Ross A, Luers K, Cieslar C, Rudolph R, Holak TA. 1994. Structure and dynamics of the human granulocyte colony-stimulating factor determined by NMR spectroscopy. Loop mobility in a four-helix-bundle protein. *Biochemistry 33*:8453-8463.